Technical Paper

ISSN 1997-1400 Int. J. Pavement Res. Technol. 4(4):244-251

Fracture Characterization of Roller Compacted Concrete Mixtures with Blast Furnace Slag and Industrial Sand

Maria C. F. Albuquerque[1], José T. Balbo[2+], Eduardo C. Sansone[2], and Paulo C. Pinto[2]

Abstract: The global energy crisis and growing environmental concerns have prompted manufacturers in general to intensify their efforts to reuse the by-products and wastes they generate. In metallurgy, steel production generates dross in the form of slag. In the present study, roller-compacted concrete (RCC) mixtures were prepared and the sand fraction was composed with industrial sand and granulated blast furnace slag. The influence of these different fine aggregates was analyzed based on the compaction parameters (moisture and dry unit weight), indirect tensile strength, flexural strength, and modulus of elasticity. Toughness and fracture tests were carried out and *R*-curve was determined for the mixtures. It was found that the RCC mixtures containing slag required larger amounts of water for compaction, presented drops in tensile strength and modulus of elasticity as well as increased the mean values of propagation energy in little amount. Both the reference RCC and the slag RCC presented a consistently upward *R*-curve and, in absolute values, showed a better *R*-curve and K_R performance than conventional and high-strength concretes previously studied in the literature. This is very important for paving purposes since a material with such a behavior shows greater resistance to catastrophic crack propagation, thus extending the service life of pavement layers.

***Key words**: Fracture mechanics, Granulated blast furnace slag, Roller-compacted concrete, Tensile strength, Toughness.*

Introduction

Environment protection has been added definitely to transportation infrastructure agenda. The reuse of wastes and by-products today in road construction is a crucial issue in improving environmental protection, since it reduces the consumption of natural resources and minimizes environmental impacts caused by the disposal of these wastes.

The manufacture of Portland cement cannot be considered ecologically correct since it consumes non-renewable natural resources and produces local environmental impacts resulting from the exploitation of limestone deposits. In its efforts to follow the concept of sustainability, the cement industry has implemented several strategies involving the use of by- products in the production of hydraulic binders. Efforts have also focused on using alternative aggregates within the concrete production cycle to help mitigating impacts caused by the exploitation of rock and sand deposits.

Aggregates may occupy up to 80% of the volume of concrete. Without the alternative of recycled aggregates, the global concrete industry would consume from 8 to 12 billion tons of natural aggregates per year besides 2010. This level of consumption would cause huge environmental impacts [1].

Therefore, the use of by-products as alternative aggregates in civil construction has become increasingly popular. Recycled materials are generally used in concrete to substitute fine or coarse aggregates or to act as cement additives. Many waste materials are used in the manufacture of concrete. One of these materials is granulated blast furnace slag, which has long been employed in the fabrication of hydraulic binder by grounding it to a fine powder with chemical components comparable to grounded clinkers.

Granulated slag originates from the production of pig iron in blast furnaces as a by-product of metallurgical processes. It derives from a combination, under specific conditions, of the minerals contained in iron ore and in foundry coke and flux ashes. During the smelting process (at ~1500°C) the metals in the liquid state are separated from the non-metallic fraction that forms the slag (less dense), which contains all the undesirable impurities and solidifies upon cooling.

The final destination of the slag as a construction material depends initially on its cooling process (the determining factor of the material's reactivity). Consisting mostly of calcium alumina-silicates, its glassy structure and high reactivity, which are essential requirements for its use as hydraulic binder, are obtained by rapid cooling in water. Prior to milling, when it is used for the fabrication of hydraulic binder, slag has a grain size and appearance resembling those of river sand, with a diameter of 0.2 to 8 mm.

Although metallurgical industry generates abundant stockpiles of granulated blast furnace slag, not all such slag is used for hydraulic binder production, thus generating a major environmental liability as a result of the open-air stockpiling of this material.

This study examined the mechanical properties of dry compacted concrete (as roller compacted concrete) using granulated blast furnace slag in substitution of fine aggregate (sand). The results obtained were compared with those of concrete manufactured with natural sands with a view to its application in paving.

Among the mechanical properties of RCC, crack propagation resistance described through the *R*-curve was crucial to understand effects of the slag san on the concrete. A material with an upward *R*-curve is more resistant to catastrophic crack propagation, what increases its fatigue life under dynamic loads.

RCC has innumerable applications in floor construction, highway

[1] State University of São Paulo, Dept. of Civil Engineering, Alameda Bahia, 550, Norte, 15385-000 Ilha Solteira, SP, Brazil.
[2] University of São Paulo, School of Engineering, Avenida Professor Almeida Prado, 83, 05508-900, São Paulo, Brazil.
[+] Corresponding Author: E-mail jotbalbo@usp.br
Note: Submitted December 2, 2010; Revised February 3, 2011; Accepted February 7, 2011.

Table 1. Characterization of the Crushed Stone Aggregates.

Parameter	Fine Aggregate	Medium Aggregate	Coarse Aggregate
Maximum Size (mm)	2.4	9.5	19
Fineness Modulus	3.507*	6.814	7.967
Specific Weight (g/cm³)	2.620	2.708	2.682
Unit Dry Weight (g/cm³)	1.630	1.390	1.430

* the studied RCC is a dry concrete not following restrictions for FM as suggested by ASTM C33.

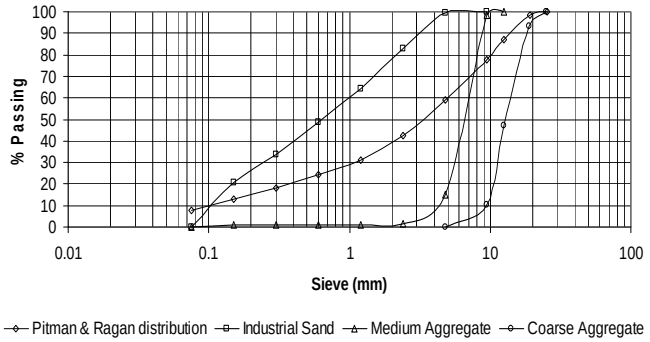

Fig. 1. Size Distribution Curves of Natural Crushed Materials.

pavements and dams [2], and transportation engineering is one of the major areas of natural resource exploitation, causing environmental impacts through its infrastructure works. On the other hand, there is a strong potential for the use of various types of by-products as blast furnace slag in these pavement base layer material, allowing for the final disposal of wastes, mitigating impacts of stock piles of industries. However, the field of application of RCC with slag sands is many times limited for applications in transportation systems and civil construction activities close to the surroundings of the metallurgical industries.

Materials used for RCC Fracture Tests

Industrial Sand, Slag and Hydraulic Binder

The RCC mixtures were prepared with crushed stones (coarse and medium aggregates) as well as fine crushed stone (called also as industrial sand) for the fine fraction proceeded from a granite stone quarry in São Paulo city. The hydraulic binder was the blended ground slag (70%) and Portland clinker (30%) designated by CP III–RS-40 type cement in Brazil. The mixing water came from the São Paulo city (potable) water supply company. Table 1 lists the data characterizing the natural materials, while Fig. 1 depicts the grains size distribution curve for the crushed (virgin) materials as well as the mixture size distribution which was based on the size distributions suggested by Pitman & Ragan [3] in order to achieve low shrinkage RCC mixtures.

The slag used in this research was collected from stockpiles of the material at the Santa Helena cement plant (120 km far from São Paulo city) prior to milling, in its open-air storage conditions. Two slag samples were subjected to a sieving analysis to ascertain their homogeneity, as shown in Fig. 2. In addition, this material was

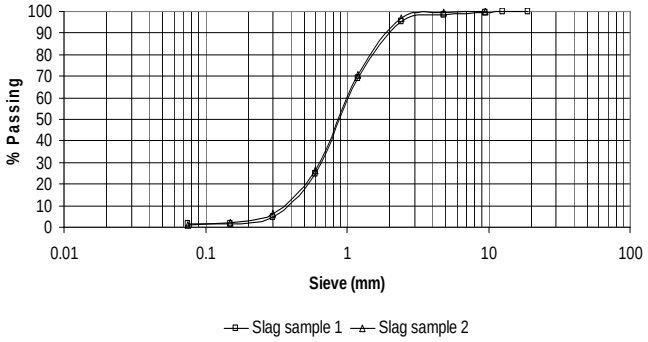

Fig. 2. Size Distribution of Collected Slag Samples.

Table 2. Physical Characterization of the Granulated Blast Furnace Slag Sand.

Parameter	Unit	Value
Characteristic Maximum Dimension	mm	2.4
Fineness Modulus	-	4.05
Content of Powder Material Above # 200 Sieve	%	0.00
Clay Lump Content	%	0.016
Specific Weight	g/cm³	2.341
Unit Mass	g/cm³	1.290
Organic Impurities	-	Lighter than Standard Solution

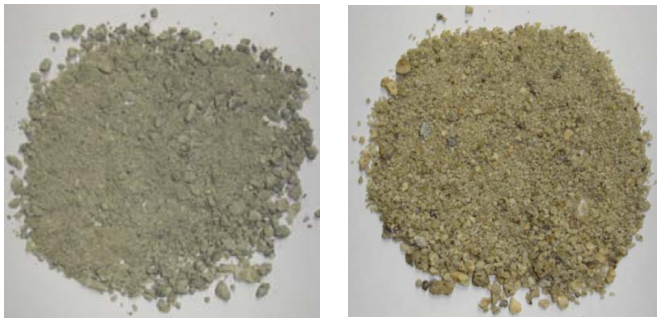

Fig. 3. Industrial Sand (Left) and Granulated Blast Furnace Slag (Right).

characterized physically by means of several laboratory tests, whose results are described in Table 2. Fig. 3 shows samples of industrial sand and slag used for RCC mixtures.

Preparation of RCC Specimens

A tensile strength of 2.5 N/mm² (splitting tensile test) was established as the goal for the RCC of reference in which crushed fine stone was used as fine aggregate. Prior to preparing the test specimens the optimal moisture content was determined by means of Proctor compaction test. The reference RCCs were mixed consummating 90, 110 and 130 kg of cement per cubic meter of concrete in order to define the cement content enough to reach 2.5 N/mm^2 tensile strength (split test). The RCCs were compacted in cylindrical (100 mm x 200 mm) and prismatic (100 x 100 x 400

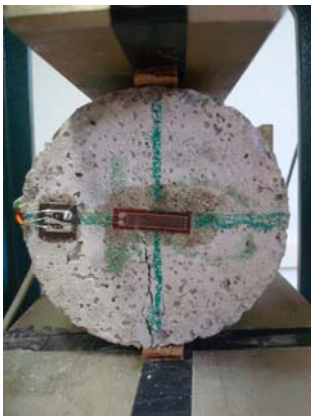

Fig. 4. Split Test with Horizontal Maximum Strain Measurements of RCC Sample.

Fig. 5. LVDT Capturing Beam Deflection During Flexural Tensile Test.

mm^3) molds using Proctor compaction criteria. The tests indicated that a consumption of 100 kg of cement per cubic meter of concrete was required to attain the previously established strength. In the RCC with slag, 100% of the sand fraction was replaced by slag (maximum diameter of 4.8 mm).

Laboratory Testing Methodology

Modulus of elasticity

The values of the modulus of elasticity were determined by two methods. The cylindrical samples were evaluated by the stress-strain curve (under traction), using the secant modulus from 5 to 70% of ultimate stress. The prismatic samples were subjected to two procedures: (a) determination of the stress-strain curve (under flexural stress), using the secant modulus from 5 to 70% of ultimate stress, and (b) by means of Mohr's analogy, based on the middle-span deflection measured with a linear variable differential transducer (LVDT) under a load equivalent to 70% of the rupture load.

Tensile Strength by Split Test (Brazilian test)

After curing the test specimens in a moist chamber up to 7 and 35 days, they were subjected to a splitting test (Brazilian test) to determine the tensile strength of each mixture; these tests followed the standard ASTM C496-90 [4]. The test specimens were instrumented with s*train gages* located at the perpendicular line to the force line to measure their horizontal tensile strain (Fig. 4).

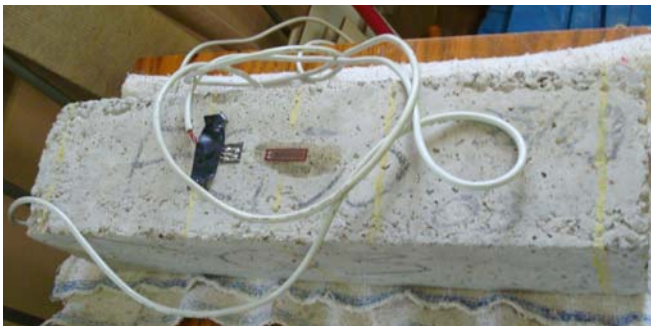

Fig. 6. Strain Gage Attached to Beam Bottom to Achieve Flexural Maximum Strain During Test.

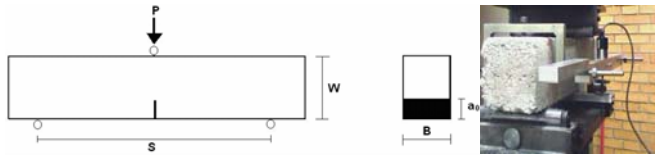

Fig. 7. Arrangement for Fracture Tests with RCC Specimens.

Bending Test for Modulus of Rupture

Flexural strength tests were carried out on prismatic test specimens, following the ASTM–C78-08 standard [5]. In these tests, a LVDT was used to measure displacement and determine the beam's mid-span deflection (Fig. 5), for subsequent calculation of the RCC modulus of elasticity. A strain gage was attached to the underside of the beam which allows the measurement of strains during the entire test up to the ultimate bending moment (Fig. 6).

Fracture and Toughness Tests

To study the fracture behavior of the reference and slag RCCs a three-point bending test was performed as illustrated in Fig. 7. The test was carried out under continuous loading and controlled displacement, using a displacement rate of 5 μm/min (this rate allows the complete load *versus* displacement curve to be determined, although it takes many hours). A servo-controlled MTS universal testing machine was used for these tests.

The crack length of the prismatic test specimens with a central notch was determined using the calibrated equation of Ferreira [6]. For this calibration, the dimensionless crack length, α_0 (crack size divided by the height of the test specimen), is valid for a length of 0.05 to 0.75. This calibration also requires test specimens with a square section, i.e., height equal to width ($W = B$), and in the testing scheme, the distance between supports, the span S, should be three times greater than the height. The test specimens (Fig. 7) had the following dimensions: 100 mm height; 100 mm width; 300 mm span; 400 mm length and a notch of 0.25 mm. The notch size was determined experimentally in order to find the lowest value at which stable crack propagation was attained.

Stress Intensity Factor (K_I)

The value of K_I is determined as a function of load, sample dimensions and crack length, according to Eq. (1) [6]:

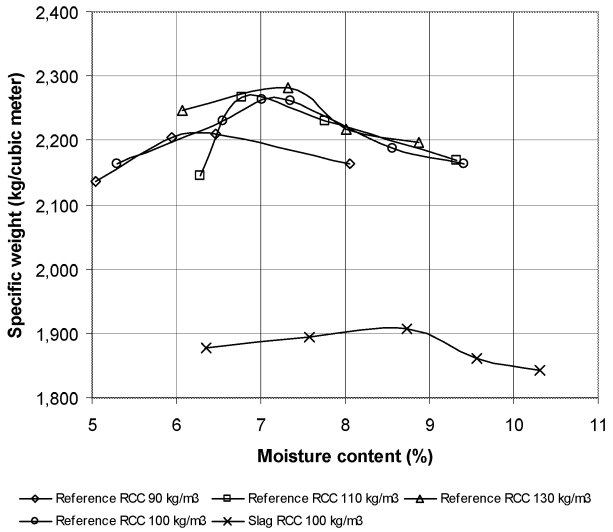

Fig. 8. Compaction Curves for the Reference RCC (with Industrial Sand) and Slag RCC.

$$K_I = \frac{1.5 \cdot P \cdot S \cdot (\pi \cdot a)^{1/2}}{B \cdot W^{1/2}} f(\alpha) \quad (1)$$

where P is the load applied (in Newton); B (beam width), W (beam height) and S (beam span) are in mm, a is the instantaneous crack length in m, and $\alpha = a/W$ is the normalized crack length for height W, with K_I obtained in MPa.(m)$^{1/2}$.

Instantaneous Crack Length (a)

The ratio of load-line displacement to applied load is given by [6]:

$$\delta = \frac{1.5 \cdot P \cdot S^2}{B \cdot W^2 \cdot E} V(\alpha) \quad (2)$$

where E is the modulus of elasticity in MPa and $V(\alpha)$ is an independent dimensionless function that depends on the test geometry, valid for $B = W$.

For a prismatic beam with $S/W = 3$, subjected to the three-point bending configuration, the dimensionless functions $f(\alpha)$ – referred to Eq. (1) = and $V(\alpha)$ can be calculated in the interval of $0.05 \leq \alpha \leq 0.75$, using the following equation:

$$f(a) \text{ or } V(a) = ia^5 + ja^4 + ka^3 + la^2 + ma + n \quad (3)$$

where α is equal to a/W and the coefficients i, j, k, l, m and n can be defined through numerical calibration for a specific sample geometry, assuming different values for functions $f(\alpha)$ and $V(\alpha)$, as for instance they are supplied by Ferreira [6].

Resistance to Quasi-Static Crack Propagation (R)

In the case of materials whose R-curve is upward sloping and which are in the condition of quasi-static crack propagation, R (crack propagation resistance) can be calculated from its relation with the instantaneous stress intensity factor at the tip of the crack. Therefore, R can be found based on linear elastic fracture mechanics (LEFM), according to Irwin [7], as follows:

$$R = \frac{K_I^2}{E} \quad (4)$$

Total Fracture Energy (γ_{wof})

A criterion to determine the reliable R values is to compare the mean value of R, R_{mean}, and the total fracture energy, γ_{wof} [8-9]. To apply this criterion, the value of R_{mean} was calculated using the following relation:

$$R_{mean} = \left(\left(\frac{1}{a_f - a_0} \right) \right)_{a0}^{af} \int R(a) da \quad (5)$$

where a_f is the final crack length with stable propagation in the valid interval ($\alpha \leq 0.75$) and a_0 is the original notch length, whereas $R(a)$ is the resistance to quasi-static crack propagation as shown in Eq. (4) as a function of the crack length itself.

The value of $2\gamma_{wof}$ was calculated from the area of stable propagation of the P versus d (Force versus displacement curve), in the interval valid for α, considering that there was no permanent deformation. Determination of the total fracture energy required calculating the work carried out by the machine on the test specimen, according to Eq. (6) below [10], but considering the interval valid for α. To this end, the integral of the load *versus* displacement curve was calculated using the computational program Origin 6.0. The integral of this curve indicates the total energy. The fracture energy was determined by subtracting the elastic energy from the total energy. The elastic energy was calculated considering no permanent deformation, i.e., by subtracting the triangle formed by the last point on the P x d curve in the elastic part (before crack propagation), the last corresponding displacement point and the origin of the P x d curve. The value of A (crack area within the propagation length) in Eq. (6) below was calculated from Eq. (3) ($\alpha = a/W$), multiplying it by the width, B, of the test specimen.

$$r_{wof} = \frac{(Area\ under\ a\ curve\ P\ x\ d)}{2A} \gamma_{wof} \quad (6)$$

Presentation and Analysis of Results

Compaction Tests

The results obtained in the compaction tests for the RCC with and without slag are presented in Fig. 8 and one can infer that consistently moisture content and dry density increase along with cement consumption growing. The moisture requirement is indeed a need when fine hydraulic binder powder amounts increases within the mixtures; this behavior was expected, since cement contains the finest particles of RCC, which increase the surface area, thus requiring more water to cover the cement particles. On the other hand cement specific weight compensates for the dry density. The

Table 3. RCCs Tensile Strength for Mixtures with 100% Industrial Sand and 100% Slag Sand.

Mixture	Type of Tensile Test	Number of Samples	Curing Age (Days)	Ultimate stress (N/mm^2)
Reference RCC (Cement Content of 100 kg/m^3)	Split	3	7	1.45 ± 0.07
	Bending	3	7	2.31 ± 0.04
	Split	6	35	2.45 ±0.08
	Bending	6	35	4.25 ± 0.32
Slag RCC (Cement content of 100 kg/m^3)	Split	6	35	1.55 ± 0.07
	Bending	6	35	2.29 ± 0.23

Table 4. Mean Values for the Modulus of Elasticity of RCC with Cement Content of 100 kg/m^3.

Mixture	Type of test	Number of Samples	Modulus of Elasticity[1] (GPa)	Modulus of Elasticity[2] (GPa)
Reference RCC	Split	6	32.1 ± 3.5	-
	Bending	6	28.6 ± 4.4	24.3 ± 3.5
Slag RCC	Split	6	21.9 ± 0.9	-
	Bending	6	19.1 ± 0,6	14.7 ± 0.9

[1] from the stress-strain curve (with strain gage); [2] from measurement of deflection (with LVDT).

replacement of sand by slag changes drastically the behavior of the material under compaction, requiring almost 2% increasing in water amount and also decreasing more than 15% its specific weight due to the lower density of slag grains compared to natural aggregates.

Tensile Strength and Modulus of Mixtures

The results for strengths achieved from split and flexural tests are shown in Table 3. The decision for using five weeks as strength measurement age was to enlarge the curing time of the specimens molded with blended cement (slag-Portland cement). Comparing the 35 days resistances it can be concluded that the desired 2.5 N/mm^2 required tensile strength for the RCC was barely achieved using the cement content of 100 kg/m^3. Summarizing, about 40% of strength loss (in tensile split test) was perceived with the replacement of industrial sand by granulated slag. The loss in term of flexural strength was up to 50%. Consistently the strength falls down with the loss of specific weight for the dry concretes. The higher values of indirect tensile strength and flexural strength of reference RCC than those of the slag RCC may be attributed to the more homogeneous grain size of industrial sand. The larger amounts of compaction water required for the mixtures with slag contributed for lower specific mass whereas more voids should be contained in such mixtures.

The mixtures also showed important drop in the modulus of elasticity as shown in Table 4 since it implies on less energy concentration at the crack tip reducing the opportunity of catastrophic crack propagation. The slag RCC presented drops about 35% in the values for modulus of elasticity in so far they present reduced specific weight as well as more void content: 3.9% in opposite to 2.3% for the conventional RCC; this is due to lower

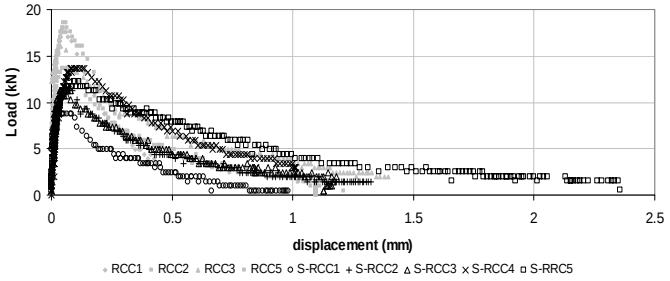

Fig. 9. Superimposition of the Load Versus Displacement Curve for the RCC with Industrial Sand and with Slag (Cement Content of 100 kg/m^3).

fineness modulus and higher w/c ratio compared to the reference RCC (Tables 1 and 2). However, the relations between modulus of elasticity (*E*) and strength (in bending, modulus of rupture or *MR*) were E/MR = 8,341 and E/MR = 6,729 for the reference RCC and the slag RCC, respectively, what could mean same advantageous behavior of the slag RCC under the point of view of pavement response: its lower rigidity compared to the reference RCC implies less tensile stresses (due to external loads) in pavement bases. Nevertheless only the toughness/fracture tests could allow claiming such a hypothesis as a feasible one.

Fracture Tests

Fig. 9 depicts the superimposed load *versus* displacement (softening) curves of the test specimens of RCC with industrial sand (RCC) and slag RCC (S-RCC), obtained from the three-point bending test performed according to the previously described methodology. One can see that the peak load is greater for the reference RCC. However, the behavior of the RCC with slag was found to be similar to that of the RCC without slag. Most of tests showed similar toughness behavior in terms of load *versus* displacement test; this similar behavior is clear from average results shown in Table 5 for the mean resistance to crack length (R_{mean}) and fracture energy per area of propagation ($2\gamma_{wof}$), respectively, 647 J/m^2 and 481 J/m^2 for the reference RCC and 671 J/m^2 and 498 J/m^2 for the slag RCC. Such results unfold no losses in terms of fracture behavior when using the alternative fine aggregate (blast furnace slag sand) in replacement to industrial sand. However one can see that individual values were more scattered for the slag RCC denoting likely more heterogeneity in slag RCC due to worst distribution of fines size dimensions (compare Fig. 1 to Fig. 2). Since these tests are time-consuming and could not be carried out on the same date, it was decided to test samples from the same batch aged for more than 120 days, when the concrete would present much lower possibilities of strength gains.

The *R*-curves are presented in two distinct ways: in Fig. 10, the crack length resistance (R) of the material as a function of normalized crack length; and Fig. 11 the K_R-curve (or K_I curve – Eq. (1)) as a function of normalized crack length.

An analysis of the results reveals that the behavior of the slag RCC closely resembled that of the reference RCC, and that the two materials showed an upward *R*-curve and K_R, with the samples 1 and 5 being the less and the most favorable behaviors for the slag RCC, respectively. The behavior of rising *R*-curves, which indicates

Table 5. Values of K_{ICIP}, R_{mean}, and $2\gamma_{wof}$ for RCC with Cement Content of 100 kg/m^3.

Mixture	Specimen #	K_{ICIP} (MPa.m$^{1/2}$)	R_{mean} (J/m^2)	$2\gamma_{wof}$ (J/m^2)
Reference RCC	1	1.94	574	426
	2	2.06	589	524
	3	1.98	809	569
	4	1.60	616	404
	Average	1.89	647	481
	Standard Deviation	0.20	109	79
Slag RCC	1	1.07	360	242
	2	1.42	567	415
	3	1.30	558	429
	4	1.71	839	697
	5	1.51	1,030	707
	Average	1.40	671	498
	Standard Deviation	0.24	263	200

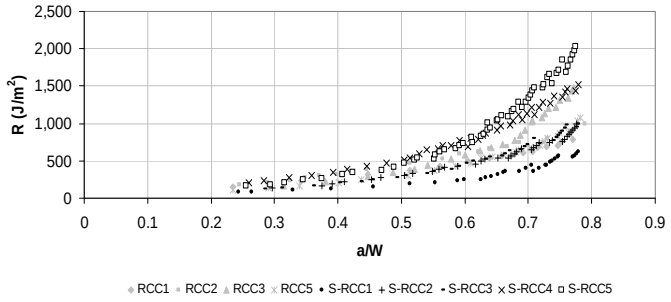

Fig. 10. Superimposition of the *R*-curves for the RCC with Industrial Sand and with Slag (Cement Content of 100 kg/m^3) as a Function of the Normalized Crack Length.

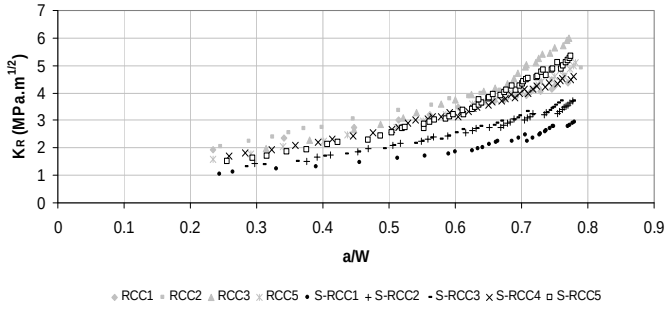

Fig. 11. K_R-curves for RCC (Cement Content of 100 kg/m^3) in Terms of Stress Intensity Factor as a Function of the Normalized Crack Length.

an increase in crack propagation resistance as the crack grows, is attributed by many authors [11, 12] to the coarse grains of the concrete and other composite materials, which enhance the adhesion between grains at the two fracture surfaces under formation, generating a mechanism that dissipates the crack propagation energy and thus causes the *R*-curve to rise.

According to Sakai [11], upward sloping *R*-curves reach a constant R value only when the process zone attains a constant and small size relative to the size of the sample. Otherwise, *R* varies with increasing crack length along its entire extent. This was the behavior observed for both RCC presented herein, i.e., a thresholdless upward *R*-curve, indicating that the process zone in this material is large in relation to the size of the sample.

Table 5 lists the values of fracture energy per area of crack propagation, $2\gamma_{wof}$, and their respective R_{mean} values. This table also shows the values of the stress intensity factor at the onset of crack propagation, which is defined here as fracture toughness at the onset of crack propagation, K_{ICIP}. An analysis of these results indicates that the K_{ICIP} value for the reference RCC was 25% higher than that for the slag RCC, and that the R_{mean} value for the slag RCC was 3% higher than that for the reference RCC. Although the reference RCC showed greater fracture toughness at the onset of crack propagation, the R_{mean} and $2\gamma_{wof}$ values were lower.

With regard to the K_{ICIP} value, it was concluded that this was higher because higher energy is required for the crack to initiate propagation, which is consistent with the higher ultimate stresses of the reference RCC (Table 3). However, after the onset of propagation, the energy required for the crack to continue propagating would be higher for the slag RCC, and therefore it presents greater resistance to catastrophic crack propagation than the reference RCC. This toughening mechanism increases the service life of pavement layers, allowing extending maintenance terms and reducing the probability of fatigue.

Comparing the mean value of R and the total fracture energy, $2\gamma_{wof}$ leads to a consistent result also obtained in former study for ceramic materials [13]: any of the tested RCC presented R_{mean} value higher than $2\gamma_{wof}$.

Comparison of Mixtures and Discussion

To compare the results of this study with former researches on concrete fracture, Figs. 12-14 show several *R*-curves obtained by other authors using the flexural test geometry. Lemaistre [12] obtained *R*-curves using the four-point bending test geometry on different concretes, and his *R*-curves were consistently upsloping. In Fig. 12, the material with largest grain size is the MChZ5 concrete (7mm) and concluded that it was not easily evident to differentiate the studied concretes according to *R* (energy). However, by comparing the *R*-curves presented in Fig. 10 it is easy to verify the better behavior in fracture presented by the reference RCC and the slag RCC when compared to the refractory concretes studied by Lemaistre [12].

In Fig. 13 are shown *R*-curves obtained numerically for five different concretes having varying compression and tensile strengths as well as varying moduli of elasticity [6]; the numerical simulation was performed for the geometry of the three-point bending test. The extreme curves for the RCC studied are plotted against those results allowing verifying that obtained K_R parameters are consistent with the mentioned numerical study.

Nevertheless the studied RCC presented ranges of variation close or similar to other different types of concretes, in Fig. 14 the results are compared to Ferreira study [6] which presented *R*-curves for a high-strength concrete and for the same concrete reinforced with different amounts of steel fiber (40 kg/m^3 and 80 kg/m^3); these curves were obtained using the three-point bending test; the values of α are valid up to the limit of 0.7. The brittleness of high-strength

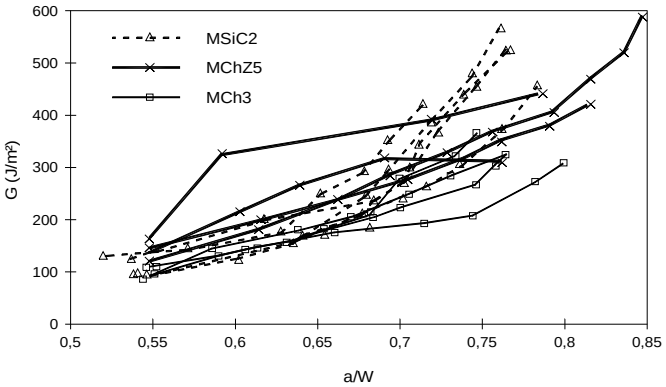

Fig. 12. G-curves for Five Different Concretes in Terms of the Strain Energy Release – *G* – in Energy/area (Adapted from Reinhardt & Xu [14]).

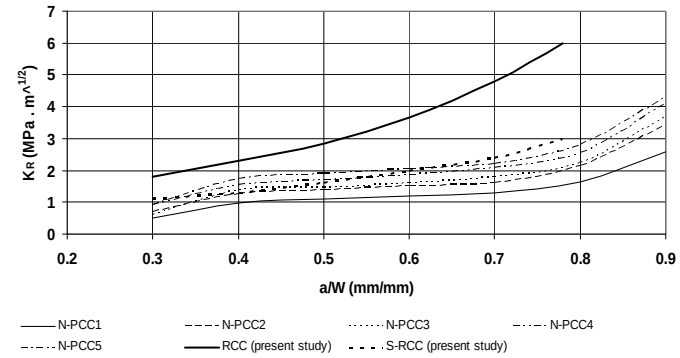

Fig. 13. K_R-curves Obtained from a High-strength Concrete by the Three-point Bending Test (Adapted from Ferreira [6]).

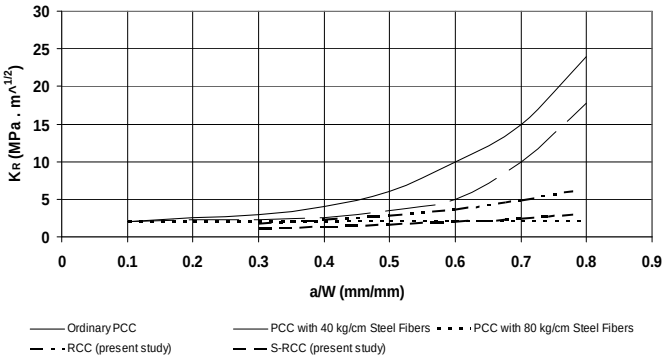

Fig. 14. K_R-curves Obtained from the High-strength Concrete Shown in Fig. 13, of the same Concrete with the Addition of 40 kg/m^3 and 80 kg/m^3 of Steel Fiber (Adapted from Ferreira [6]).

concretes makes RCC to be more resistant to fracture at some instance.

The behavior of the *R*-curve for the studied reference and slag RCC, upsloping *R*-curve, is consistent with coarse-grained materials, such as the concrete studied by Lemaistre [12], Reinhart and Xu [14] and by Ferreira [6]. These authors also consistently obtained thresholdless upsloping *R*-curves, with the exception of the high-strength concrete produced by Ferreira [6], a material with a much higher strength and much greater brittleness, whose process zone was therefore probably smaller.

Mazzei *et al.* [15] states that the shape of the consistently upward *R*-curve is due to the calibration equation for the flexural test. However, this does not seem to be the case of the *R*-curves obtained in the present study, since the equation used here was the one deduced by Ferreira [6], who obtained an upsloping *R*-curve with a threshold for the high-strength concrete without fiber.

Comparing the absolute values of the *R*-curves (Figs. 10 and 11) and K_R presented in this study (Table 5) against those depicted in Figs. 12 to 14, it can be stated that the reference RCC showed a better performance of crack opening resistance than the conventional and high-resistance concretes, with the exception of the steel fiber-reinforced high-strength concrete produced by Ferreira [6]. The same hold true for the slag RCC. It should be kept in mind that the values should be analyzed for α up to 0.7. As for the criterion for evaluating the reliability of the values of *R*, both the reference and slag RCC presented a mean R higher than the $2\gamma_{wof}$.

The obtained result of lower modulus of elasticity/strength ratio for the slag RCC in combination with the higher energy required for the slag RCC to proceed to catastrophic crack propagation are, therefore, good parameters favoring possible better performance of slag RCC as pavement layers, reducing its probability of fatigue in view of results for the reference RCC.

Conclusions

The laboratory studies to evaluate the mechanical properties of the RCC containing slag led to the conclusions as follows below.

Compared to the reference RCC, the slag RCC presented a drop in its modulus of elasticity, as well as in dry density, indirect tensile strength and flexural strength. In other words, from the standpoint of static parameters, the incorporation of slag caused significant decreases in physical and mechanical parameters, which would eventually offset each other in terms of structural responses as pavement layers. However, the modulus of elasticity/strength ratio showed favorable results for the behavior of slag RCC as pavement base layer if one considers that, for the same pavement structure thicknesses and the same loads, tensile stresses can be reduced, what is favorable in terms of durability.

Toughness-fracture tests were then performed to better clarify and avoid jeopardizing the use of slag (as sand) in the RCC mixtures. Both the RCC mixtures presented a consistently upsloping *R*-curve, i.e., thresholdless. This was more likely due to the relatively large size of the process zone relative to the size of the test specimen and not due to the equation of K for the flexural test.

The reference RCC presented 3% lower mean values of R_{mean} than the slag RCC and higher values of onset of crack propagation. This occurred likely because its higher strength ensured higher values of toughness at the onset of crack propagation. However, more energy is required for a crack to continue propagating in the slag RCC. This toughening mechanism increases the service life of the pavement, allowing extending maintenance terms and reducing the probability of fatigue.

It was also found that the two concretes of this study showed toughening mechanisms due to the upsloping *R*-curve. Although the dimensions of the test specimens were small in relation to the process zone, it is unfeasible to test larger specimens in order to obtain an upsloping *R*-curve which reaches a threshold. However, the objective of this study was to compare these materials in order to reach a conclusion about the action of energy dissipation

mechanisms. This was done by ensuring that the same test conditions were kept and if changes in the shape of the *R*-curve occurred, they would not be the result of changes in the test condition.

In absolute values, all the RCC mixtures presented higher crack propagation resistance than conventional or high strength concretes, during the process of crack growth; i.e., they showed a better *R*-curve and K_R performance than conventional and high-strength concretes previously studied and reported in the literature, with the exception of steel fiber-reinforced high-strength concrete. This is very important in paving, because a material with this behavior shows fewer propensities for catastrophic crack propagation (less probability of fatigue) and therefore increases the service life of the pavement layer (for instance, bases and sub-bases underneath asphalt layers). Although the slag RCC presented lower values of strength and K_{ICIP} than the reference RCC, the values of strength would still be adequate for pavement layers. The slightly higher values of R_{mean} and $2\gamma_{wof}$ for the slag RCC indicate an advantage for increasing the pavement's service life. Moreover, the upsloping *R*-curves of the concretes, with higher absolute values than those displayed by conventional concretes, were clearly favorable. Nevertheless, this little increment of fracture energy to slag RCC came along with more scattered individual results that could be explained by the worst fine grain size distribution of the slag RCC (the industrial sand contains 40% of retaining grains between 1 and 5 mm against 40% of retaining grains between 1 and 3 mm in the slag sand).

The incorporation of granulated blast furnace slag, which represents one of the problems of disposal of solid wastes in the environment, therefore showed to be feasible for use in RCC as a substitute for natural or industrial sands, and hence saving energy for exploration and transportation of fine aggregates in areas where granulated slag is available, indicating that this material deserves further study aiming at its large scale application. Such future investigation should likely consider alkali-silica reaction (ASR) issues mostly when no blended cements with mineral pozzolans addition are employed to concrete manufacture; also strict control of K^+ and Na^+ contents in hydraulic binders shall be addressed in pavement construction to ensure avoiding ASR in medium or long term performance. This deleterious reaction drastically decreases the modulus of elasticity and flexural strength of concretes inducing flexible pavement responses to loads and spoiling pavement durability. In such a situation values for parameters achieved for young concretes within the scope of the present research and results shall be not applied for pavement analysis. Also future investigation should consider more attention to the variability of slag sand sizes distribution and how it could interfere on statistical values once it was verified important scatter on toughness-fracture studies with the slag RCC.

Acknowledgments

Authors gratefully acknowledge the support from the Brazilian National Research Council (CNPq Process # 473498/2006-5) and from the Deputy Research Office of UNESP.

References

1. Tu, T.Y., Chen, Y.Y., and Hwang, C.L., (2006). Properties of HPC with Recycled Aggregates, *Cement and Concrete Research*, 36(5), pp. 943-950.
2. Atis, C.D., Sevim, U.K., Ozcan, F., Bilim, C., Karahan, O., Tanrikulu, A.H., and Eksi, A., (2004). Strength Properties of Roller Compacted Concrete Containing a Non-standard High Calcium Fly Ash, *Materials Letters*, 58(9), pp. 1446-1450.
3. Pittman, D.W., and Ragan, S.A., (1998). Drying Shrinkage of Roller-Compacted Concrete for Pavement Applications, *ACI Materials Journal*, 95(1), pp. 19-26.
4. American Society for Testing and Materials, (1993). Standard Test Method for Splitting Tensile Strength of Cylindrical Concrete Specimens, *ASTM Standard C496-90*, West Conshohocken, Philadelphia, USA.
5. American Society for Testing and Materials, (2008). Standard Test Method for Flexural Strength of Concrete (using simple beam with third-point loading), *ASTM standard C78-08*, West Conshohocken, Philadelphia, USA
6. Ferreira, L.E.T., (2007). Fracture analysis of a high-strength concrete and a high-strength steel-fiber-reinforced concrete, *Mechanics of Composite Materials*, 12(5), pp. 479-486.
7. Irwin, G. R., (1957). Analysis of stresses and strain near the end of a crack, *Journal of Applied Mechanics*, Vol. 24, p. 361.
8. Kleinlein, F.W., and Hubner, H., (1977). *R*-Curve Evaluation with Ceramic Materials at Elevated Temperatures by an Energy Approach Using Direct Observation and Compliance Calculation of the Crack Length, *Proceedings of ICF4*, Vol. 3, pp. 883, Waterloo, Canada.
9. Bornhauser, A., Kromp, K., and Pabst, R.F., (1999). Crack extension resistance based on the cohesive force in concrete, *Engineering Fracture Mechanics*, 64(5), pp. 563-587.
10. Nakayama, J., (1965). Direct Measurement of Fracture Energies of Brittle Heterogeneous Materials, *Journal of American Ceramic Society*, 48(11), pp. 583-587.
11. Sakai, M., (1987). Fracture Mechanics of Refractory Materials, *Taikabutsu Overseas*, 8(2), pp. 4-12.
12. Lemaistre, H., (1998). Étude des Propriétés Thermomécaniques de Divers Réfractaires, *PhD Dissertation*, École Doctorale Matériaux, Institut National de Sciences Appliquées, Lyon (in French).
13. Albuquerque, M.C.F., and Rodrigues, J.A., (2006). Characteristics of the double-torsion test to determine the *R*-curve of ceramic materials, *Materials Research*, 9(4), pp. 361-368.
14. Reinhardt, H.W., and Xu, S., (1999). Crack Extension Resistance Base on the Cohesive Force in Concrete, *Engineering Fracture Mechanics*, Vol. 64, pp. 563-587.
15. Mazzei, A.C., Rodrigues, J.A., and Pandolfelli, V.C., (2000). Alumina-mullite-zirconia composites obtained by reaction sintering - Part II. *R*-curve behavior, *Journal of Materials Science*, 35(11), pp. 2815-2824.